Research paper





# 3D DLP-printed cannabinoid microneedles patch and its pharmacokinetic evaluation in rats

# Arvind Bagde<sup>1</sup>, Keb Mosley-Kellum<sup>1</sup>, Shawn Spencer<sup>2</sup>, Mandip Singh<sup>1,\*</sup>, ©

<sup>1</sup>College of Pharmacy and Pharmaceutical Sciences, Florida A&M University, Tallahassee, FL, United States

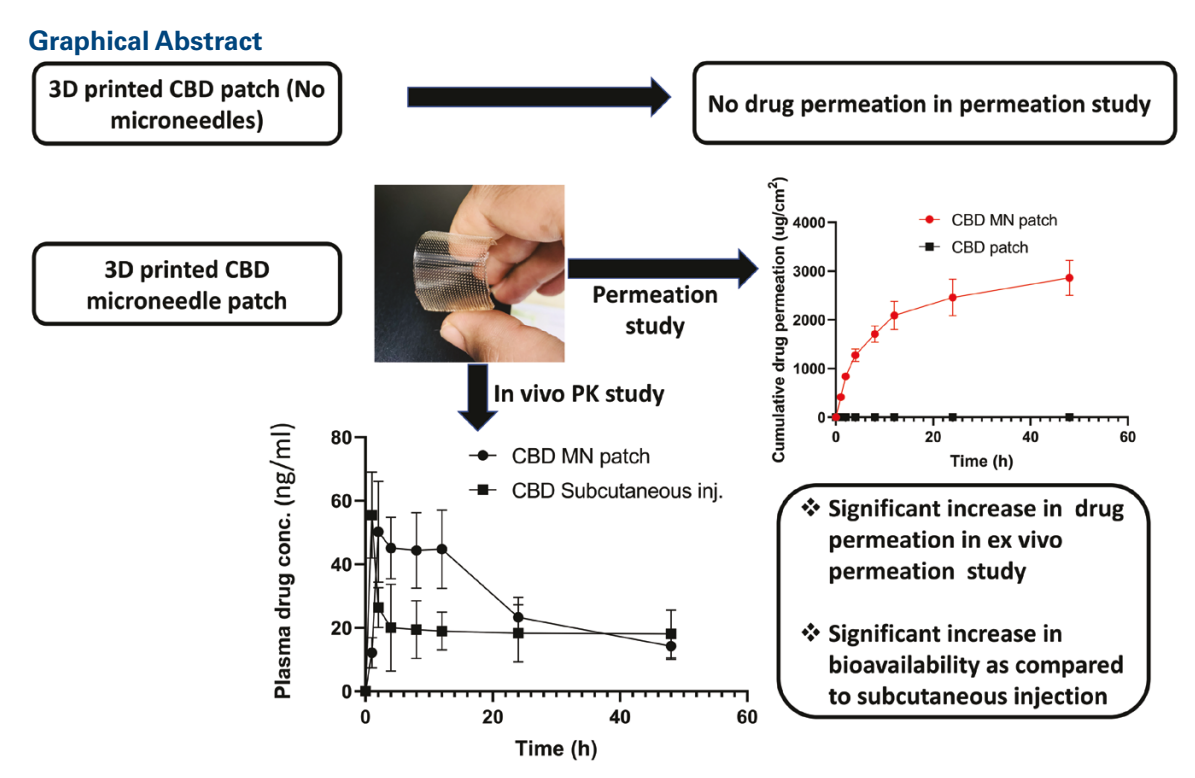
#### **Abstract**

**Objective:** The objective of the present study was to enhance the bioavailability of cannabidiol (CBD) using 3D Digital Light Processing (DLP)-printed microneedle (MN) transdermal drug delivery system.

**Methods:** CBD MN patch was fabricated and optimized using 3D DLP printing using CBD (8% w/v), Lithium phenyl-2,4,6-trimethylbenzoylphosphinate (LAP) (0.49% w/v), distilled water (20% w/v), and poly (ethylene glycol) dimethacrylate 550 (PEGDAMA 550) (up to 100% w/v). CBD MNs were characterized for their morphology, mechanical strength, *in vitro* release study, *ex vivo* permeation study, and *in vivo* pharmacokinetic (PK) profile.

**Key findings:** Microscopic images showed that sharp CBD MNs with a height of ~800 μm, base diameter of ~250 μm, and tip with a radius of curvature (RoC) of ~15 μm were successfully printed using optimized printing parameters. Mechanical strength studies showed no significant deformation in the morphology of CBD MNs even after applying 0.5N/needle force. *Ex vivo* permeation study showed significant (P < .0001) permeation of CBD in the receiving media as compared to CBD patch (control). *In vivo* PK study showed significantly (P < .05) enhanced bioavailability in the case of CBD MN patch as compared to CBD subcutaneous inj. (control).

Conclusion: Overall, systemic absorption of CBD was significantly enhanced using 3D-printed MN drug delivery system.



Keywords: dissolving microneedles; CBD; 3D printing; photoinitiator; DLP

PCOM School of Pharmacy, Philadelphia College of Osteopathic Medicine (PCOM), Philadelphia, PA 19131, United States

<sup>\*</sup>Correspondence: Department of Pharmaceutics, College of Pharmacy and Pharmaceutical Sciences, Florida A&M University, Tallahassee, FL 32307, United States. E-mail: mandip.sachdeva@gmail.com

# Introduction

In recent years, there has been an increasing demand for novel and efficient drug delivery systems to overcome the limitations of traditional routes such as oral, intravenous, and intramuscular administration. Transdermal drug delivery offers numerous advantages, including non-invasive application, controlled release kinetics, reduced systemic side effects, and improved patient compliance. Among the various transdermal delivery methods, micro-needle patches have emerged as a promising technology, revolutionizing the field of drug delivery. These patches consist of microscopic needles capable of penetrating the skin's epidermal stratum corneum layer to facilitate the controlled delivery of therapeutic agents [1–3]. The emergence of 3D printing in the field of microneedle patch fabrication has led to significant progress in recent years. Researchers have extensively investigated the drug delivery efficiency of 3D-printed micro-needle patches by examining factors such as drug release kinetics, drug loading capacity, and skin penetration capabilities. In vitro and in vivo studies have demonstrated the successful delivery of various therapeutics using 3D-printed micro-needle patches, highlighting their potential as a promising alternative to traditional drug delivery methods [4, 5].

Within the manufacturing domain, two primary approaches are commonly used to classify 3D printing techniques: layerby-layer and point-by-point methods. The point-by-point printing technology uses accurate point-by-point printing to build a 3D MN structure. Within this category, notable 3D printing processes that are used to produce MN are fused deposition molding (FDM), direct metal laser sintering, twophoton polymerization, and laser stereolithography (laser SLA). On the other hand, photosensitive material is gradually solidified, one layer at a time, during the layer-by-layer printing process. Several well-known 3D printing technologies that use the layer-by-layer method include vat polymerization for LCDs, digital light processing (DLP), static optical projection lithography, continuous liquid interface production, and magnetorheological drawing lithography [6]. Researchers used FDM 3D printing technology to fabricate biodegradable MN patches. The patches were examined for skin penetration and drug release kinetics after being loaded with a model drug. The outcomes demonstrated a prolonged release of the drug over a number of days, underscoring the potential of 3D-printed MN patches for continuous drug delivery [6, 7]. SLA 3D printing was used to design and fabricate a hollow micro-needle array capable of encapsulating a higher drug volume. The hollow micro-needle patches exhibited promising potential for delivering high-dose therapeutics [8, 9]. Dissolving MNs are manufactured by incorporating the active pharmaceutical ingredients (APIs) within polymers. Once they pierce through the outer layer of the skin (stratum corneum), the polymer that constitutes the needle structure dissolves, subsequently releasing the contained drug [10].

Cannabinoids, including CBD, are reported to possess anti-inflammatory, anti-necrotic, and anti-oxidative effects, indicating considerable therapeutic potential for patients with conditions such as Alzheimer's disease, epilepsy, Parkinson's disease, and multiple sclerosis [11–14]. However, CBD exhibits poor bioavailability (13–19%) when orally administered because of numerous factors such as first-pass metabolism, low aqueous solubility (2–10  $\mu$ g/ml in water), and high lipophilicity (log P values of > 5) [11, 13]. Additionally, it

possesses weak acidic properties (pKa 9.1), a melting point of 67°C, and a molar mass of 314 g/mol. Consequently, CBD falls under Class II of the Biopharmaceutics Classification System, indicating it is poorly water-soluble yet highly permeable [15]. Therefore, MN transdermal delivery can be the ideal route for enhancing the bioavailability of CBD as it circumvents the first-pass metabolism unlike the oral route [16]. There are studies reported in the literature on CBD transdermal delivery using the micromolded MN method. In a study by Shi et al., effervescent CBD solid dispersion-doped dissolving MNs (Ef/CBD-SD@DMNs) composed of the combined effervescent components (CaCO3 and NaHCO3) and CBD-based solid dispersion (CBD-SD) were fabricated [17]. Muresan et al. developed polymer-coated nanoparticles (NPs) containing cannabidiol (CBD) or olaparib (OLA) MN patch using the micromolding method for local drug delivery to the brain [18]. To the best of our knowledge, ours is the first study demonstrating CBD delivery using 3D DLP-printed methodology with enhanced transdermal permeation and bioavailability. The present 3D printing technique is a continuous single-step manufacturing process that bypasses multiple steps involved in conventional micromolding techniques. In our previous study, we have developed dissolving ibuprofen MN patch using 3D DLP technology in a continuous single step [16]. The objective of the present study was to develop CBD MN patches to enhance its bioavailability using our previously optimized 3D DLP printing technology.

# Materials and methods

#### Materials

The 3M Tegaderm TM waterproof transparent dressing and the Micro DLP 3D printer were acquired from VWR, USA, and Kudo3D, CA, USA, respectively. LAP and PEGDAMA 550 were procured from Sigma Aldrich, MO, USA. CBD was purchased from Open Book Extracts, NC, USA.

# Animals

Sprague Dawley (SD) rats were obtained from Charles River Laboratories in Wilmington, Massachusetts, for use in in vivo PK studies. The rats were housed in cages with appropriate bedding with controlled conditions, including a temperature of 22 ± 2°C, a 12:12 hour light-dark cycle, and relative humidity kept at  $50 \pm 15\%$ . Following the recommendations in the "Guide for the Care and Use of Laboratory Animals" and the criteria established by the Association for Assessment and Accreditation of Laboratory Animal Care, these rats were housed at Florida A&M University. Before commencing any experiments, the rats underwent a one-week acclimatization period in the laboratory conditions [19, 20]. Additionally, Florida A&M University's Institutional Animal Care and Use Committee (IACUC) approved all animal protocols used in this study (protocol approval no. 019-07 and approval date: May 10, 2021).

# Methods

# Formulation of CBD resin formulation

CBD resin formulation was prepared using our previously established method [16]. Briefly, 20% w/v water was used to dissolve 0.49% w/v of LAP. After adding the LAP solution, PEGDAMA 550 (up to 100% w/v) was vortexed for 1 minute. In order to allow the water to evaporate, the formulation was

then placed on a hotplate stirrer at 42°C for 45–60 minutes. 10% w/v of water remained in the resin formulation following the evaporation. CBD was then added to the resin and vortexed until it totally dissolved. Prior to formulation optimization, studies on the solubility of CBD were carried out. We found that turbidity and CBD precipitation occurred in the formulation when the concentration of CBD exceeded 8% w/v, indicating that 8% w/v was the highest concentration of soluble CBD in the formulation.

#### 3D printing of CBD MN patch

Autodesk Fusion 360 was used to create the CBD MN patch STL file. It was then imported into the Micro DLP 3D printer after being sliced at 15  $\mu$ m in the Kudo3D print job preparation program. The CBD MN patches were printed with an LED current of 125 (5.86 mA/unit), a slice thickness of 25  $\mu$ m, and an exposure time of 4–5 seconds. The printed MN patches were cured in a UV curing chamber at 23°C for 15 minutes after being cleaned in 70% IPA. After that, optical microscopy was used to examine the morphology of the printed patch [16].

## Drug content analysis

Briefly, CBD MN patches and CBD patches (no MN) were cut into small pieces and dissolved in acetonitrile: water (80:20) solvent. Samples were then vortexed and sonicated for 1 hour each to extract the drug from CBD MN patches and CBD patches (no MN). Samples were then centrifuged at 16,000 RPM for 15 minutes. Finally, the supernatant was collected and analyzed for drug content using the LC-MS method.

# Mechanical strength

#### Manual characterization

The MN patch was manually pressed with thumb pressure to human dermatomed skin for 60 seconds and examined under the optical microscope to determine whether any pores had formed on the skin. The ability of MNs to break the skin's stratum corneum layer without causing damages to the MN structure was used to determine the mechanical strength of MNs [21].

# Texture analyzer characterization

Briefly, adhesive tape was used to affix the MN patch to the moving probe (TA XT Texture Analyzer, Stable-Micro Systems, USA). Next, the patch was pressed on the human dermatomed skin at a rate of 0.5 mm/sec for 30 seconds using a flat aluminum block and compression forces of 0.1, 0.2, 0.3, 0.4, and 0.5 N/needle. The pre-test and post-test speeds were both fixed at 0.5 mm/sec. Before and after applying the force, MN height was measured, and any changes in height or deformation were noted [16, 22].

#### In vitro release study

Phosphate buffer (pH 7.4) with 25% ethanol and 5% Tween 80 was used as a dissolution medium for the *in vitro* study of CBD MN patches. Briefly, a beaker containing 20 ml of dissolution medium was kept on a magnetic hotplate at 350 rpm at 37°C. CBD MN patches and CBD patches (no MN) were added to the release medium. Samples were withdrawn at 1, 2, 4, 6, 8, 12, and 24 hours. At each sampling time, fresh 20 ml of dissolution medium was replaced in the beaker [23]. Samples were then analyzed using the LCMS method.

#### Ex vivo permeation testing using human skin

We acquired human skin from the New York Firefighters Skin Bank at New York Presbyterian Hospital, NY, USA, which had been dermatomed to a thickness of  $0.5 \pm 0.1$  mm. This skin was kept at -80°C and transported in a 10% glycerin solution in saline. The skin was defrosted and rinsed with distilled water for about 45 minutes to get rid of any extra glycerin before any experiments were conducted. Our laboratory has previously verified the storage and preparation methods for dermatomed human skin, confirming that the skin maintains its structural integrity to ensure accurate permeation. Additionally, the skin's integrity was meticulously evaluated through visual inspection to confirm the absence of any perforations or flaws [24–28]. The receiving compartment was filled with PBS buffer (pH 7.4), containing 25% ethanol and 5% Tween 80, and was kept at a constant temperature of  $32 \pm 0.5$ °C with continuous stirring at 300 rpm. In the experimental setup, the MN CBD patch (N = 3) and CBD patch (no MN) (N = 3) were applied to the skin manually with thumb pressure. To secure the patch in place and ensure continuous contact with the skin, sellotape was used. The skin, along with the patch, was then positioned between the donor and receiver compartments of the Franz diffusion cells from PermeGear Inc., located in Riegelsville, PA, USA. Samples were collected at time intervals of 1, 2, 4, 8, 12, 24, and 48 hours. At each sampling time point, a new release medium was introduced into receiving compartment to maintain consistency in the experiment [29]. Solubility study was conducted in various receiving media: (i) PBS buffer only (pH 7.4), (ii) PBS buffer with 5% ethanol, (iii) PBS buffer with 10% ethanol, (iv) PBS buffer with 25 % ethanol, and (v) PBS buffer with 25% ethanol and 5% Tween 80. Data showed >2 mg/ml CBD solubility in release media consisting of PBS buffer with 25% ethanol and 5% Tween 80 as compared to all other media which showed <2 mg/ml CBD solubility. Therefore, PBS buffer (pH 7.4), containing 25% ethanol and 5% Tween 80 was used as a receiving media for conducting the ex vivo permeation testing. Sink conditions were maintained throughout the experiment.

#### In vivo PK study

The animal experiments performed in this study were approved by the IACUC, Florida A&M University, Tallahassee, FL, USA. All research were conducted in accordance with this approved protocol (protocol approval no. 019-07 and approval date: May 10, 2021). Male Sprague–Dawley rats, weighing approximately 250 g, were employed to assess the transdermal efficacy of MNs in vivo. The rats underwent a 7-day acclimatization period in the laboratory prior to the experiment. To ensure uninterrupted dermal contact with the patch, the animals were anesthetized with 2–4% isoflurane in oxygen 24 hours before the experiment, and their fur was removed using an animal hair clipper. The animals were then categorized into two groups: Group 1 received a CBD MN patch, while Group 2 received CBD in dimethyl sulfoxide (DMSO). A dose of 30 mg/kg was administered to each group. The CBD patch, equipped with MNs, was applied to the rats to facilitate transdermal CBD delivery. CBD MN patches were affixed to the backs of Sprague–Dawley rats (N = 4) using 3M Tegaderm<sup>TM</sup> adhesive patches. In Group 2, rats (N = 4) were administered subcutaneous injections of a CBD solution in DMSO. Blood samples were collected at specified time intervals of 1, 2, 4, 8, 12, 24, and 48 hours. To obtain plasma, the collected whole blood samples were centrifuged at 4000 rpm at 4°C. The resulting plasma samples were then stored at -80°C until they underwent analysis [30]. All the samples were then analyzed using LCMS. Upon completion of the study, an assessment was conducted to investigate whether the application of patches on the skin had induced any inflammation or damage in the rats [31]. The relative bioavailability of CBD MN patch was calculated using the following formula:

Fr = ((mean AUC)test/(mean AUC)std)  $\times$  100, Where Fr is Relative bioavailability; mean AUC<sub>test</sub> is the mean AUC of CBD MN patch group; and mean AUC<sub>std</sub> is mean AUC of CBD subcutaneous injection group [32].

#### **HPLC-MS** method

HPLC-MS analysis was conducted with a Waters e2695 separation module, QDa detector, Aquity QDa, and Waters 2998 photodiode array detector (Waters Technology Corporation, USA). A mobile phase containing 90% ACN (0.1% formic acid) and 10% water (0.1% formic acid) was used at a flow rate of 0.5 ml/min with an injection volume of 20 ul. Column temperature was set to 40°C. A reverse phase C18 column (Nova-Pak® 3.5  $\mu$ m, 3.9 × 150 mm; Waters Technology Corporation, USA) with a guard column (Symmetry®, reversed phase, C18) was used for the elution of samples. QDa was set to a mass range: 250–350 Da, positive scan, cone voltage 22V, capillary voltage (positive: 1.5 kV and Negative: 0.8 kV), SIR with mass 315 Da positive polarity, and cone voltage of 22V.

#### Linearity

The linearity was established by analyzing five CBD standard concentration in the range of 12.5, 25, 50, 100, and 200 ng/ml. All the standards were processed using solid phase extraction method using Oasis PRiME HLB 96-well  $\mu Elution$  Plate (Waters Technology Corporation, USA) with established protocol by the vendor [33]. Briefly, CBD standards with rat plasma were first diluted with 4% phosphoric acid and run in 96-well  $\mu Elution$  well plate. Further, wells consisting of CBD standards were washed with 200  $\mu l$  of Methanol:Water (5:95) solvent and finally eluted with 100  $\mu l$  of Acetonitrile (CAN): Methanol (90:10) solvent. The collected eluent was then analyzed using the HPLC-MS method. Our results showed that the calibration curve (peak intensity area vs concentration) was linear with a correlation coefficient of 0.99. The retention time was found to be 4.44 minutes.

# Accuracy

An accuracy study was conducted at three concentration levels (25, 50, and 100 ng/ml) of CBD standards and the recovery percentage was calculated. The percent recoveries were found to be  $97.49 \pm 1.34$ ,  $98.68 \pm 1.07$ , and  $98.31 \pm 1.45\%$  for 25, 50, and 100 ng/ml CBD standards, respectively.

#### Precision

The method precision was validated through intra-day and inter-day testing of CBD standards (25, 50, and 100 ng/ml concentration). The method's intra-day precision was assessed by conducting six independent assays of CBD test samples against a reference standard on the same day. Furthermore, these assessments were replicated over six consecutive days

to ascertain inter-day precision. The percentage of the relative standard deviations (%RSD) of 25, 50, and 100 ng/ml CBD standards were found to be below 3.9% and 4.5% for intraday and inter-day, respectively.

#### Detection and quantitation limits

The limit of detection (LOD) and limit of quantification (LOQ) were calculated using following equations based on the standard deviation of the response and the slope as per the ICH guidelines [34]:

 $LOD = 3.3 \times (SD \text{ of intercept/slope})$  and  $LOQ = 10 \times (SD \text{ of intercept/slope})$ 

LOD and LOQ for the CBD standards were found to be 5.26 ng/ml and 15.95 ng/ml, respectively.

#### Statistical and PK analyses

The raw data results were presented as the mean  $\pm$  standard deviation based on a minimum of three repetitions. For comparisons between two groups, Student's *t*-test analysis was employed. Significance in mean differences was determined in all experiments with \*P < .05, \*\*P < .01, and \*\*\*P < .001. PK analyses were performed using PKSolver for noncompartmental analysis and Graphpad Prism (Dotmatics, Boston, MA, USA) for user-defined model fits [35]. The mean  $\pm$  standard error was utilized to present the model fit parameters. The *in-vitro in-vivo* relationship was assessed by determining the fraction absorbed *in vivo* through noncompartmental analysis and the Wagner–Nelson method of numerical deconvolution [36].

# Results

# DLP 3D-printing of CBD-loaded MN and drug content study

Resin formulation consisting of CBD (8%w/v), LAP (0.49% w/v), water (20% w/v), and PEGDAMA 550 (up to 100% w/v) resulted in a clear transparent formulation with no sedimentation of particles. Further, the formulation produced CBD MN patches without any excessive polymerization when printed with a 25-µm slice thickness, LED current set at 125 (5.86mA/unit), and exposure time ranging from 4 to 5 seconds. Our printing results showed that our previously optimized printing parameters [16] produced sharp CBD MNs. Optical microscopic examination revealed that the MNs were manufactured with a height of approximately 800 µm, a base diameter of about 250 µm, and tips characterized by RoC close to 15 µm (Fig. 1). Results revealed that CBD MN patches and CBD patches (no MN) showed 95.36  $\pm$  2.52 and 94.77  $\pm$  3.19 % drug, respectively.

# Mechanical properties of CBD MN patch Manual characterization

Images showed that CBD MNs formed pores on the human dermatomed skin after pressing the MN patch with slight thumb pressure. Furthermore, no damage to the MN structure was observed after the application, suggesting that CBD MNs were robust to break the stratum corneum layer of the skin (Fig. 2a).

#### Texture analyzer characterization

Results demonstrated that pressing the CBD MN patch against dermatomed human skin with a probe at various

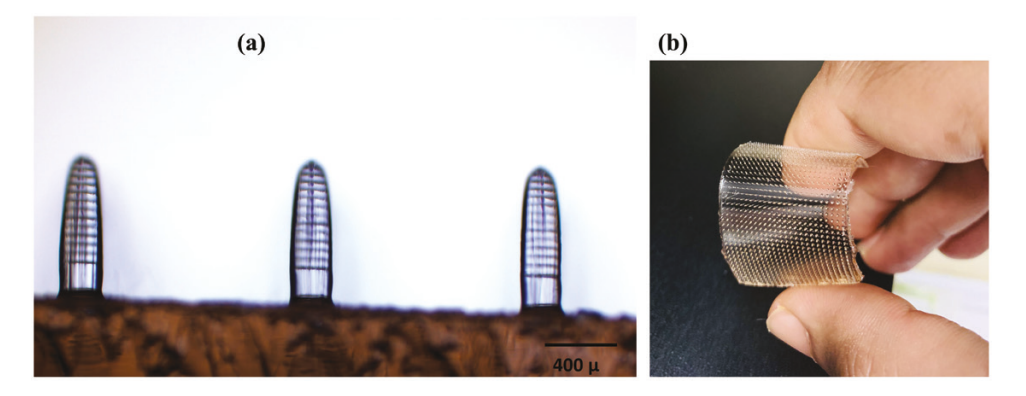


Figure 1. (a) Optical microscopic image showing cannabidiol microneedles (CBD MNs) with  $\sim$ 800  $\mu$ m height,  $\sim$ 250  $\mu$ m base diameter and tip with radius of curvature (RoC) of  $\sim$ 15  $\mu$ m; (b) cannabidiol microneedle (CBD MN) patch used in *in vivo* animal study (results are expressed in mean  $\pm$  SD [n = 3]).

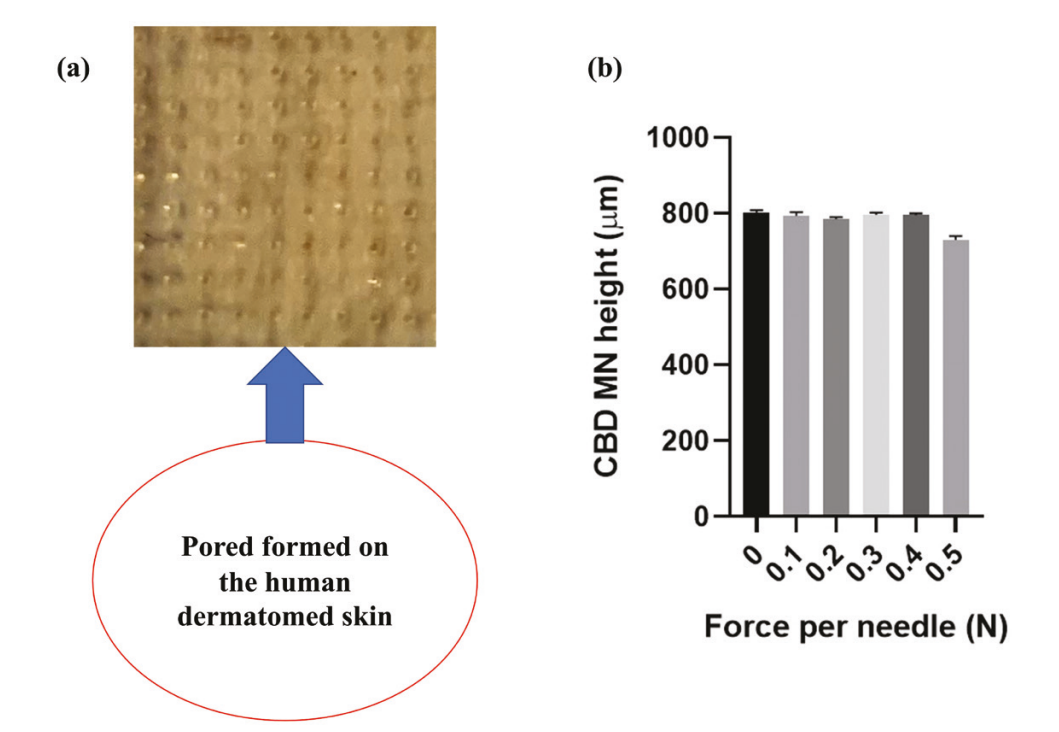


Figure 2. (a) Human skin with pores formed after the application of cannabidiol microneedles (CBD MNs); (b) mechanical strength study of cannabidiol microneedles (CBD MNs) showing no significant difference in the height of microneedles (MNs) (results are expressed in mean  $\pm$  SD [n = 3]).

forces ranging from 0.1 to 0.5 N per MN did not result in a reduction in the height of the MNs. This observation suggests that the MNs possess sufficient strength to break the epidermal layer of the skin. Moreover, microscopic images verified that the CBD MNs remained intact without breaking even after applying force of 0.5 N per MN (Fig. 2b).

#### *In vitro* release study

In vitro drug release data showed  $44.23 \pm 3.78\%$  and  $30.99 \pm 4.87\%$  drug release at 2 hours from CBD MN patch and CBD patch (no MN), respectively. Data showed increased drug release ( $79.54 \pm 8.56\%$ ) in the case of CBD MN patches as compared to CBD (no MN) patches, which showed  $66.85 \pm 3.78\%$  at the end of 24 hours. Although both the formulations contain similar concentrations of LAP and water, CBD patches with MNs showed higher drug release as compared to patches with no MNs. It was also observed that

the base diameter of CBD MNs was increased from to ~310  $\mu$ m from ~250  $\mu$ m and height decreased ~600  $\mu$ m from ~800  $\mu$ m after 2 hours (Fig. 3a).

#### Ex vivo permeation testing using human skin

Permeation data demonstrated that CBD MN patches showed significantly higher (P < .0001) CBD permeation (2861.03 ± 360.66 µg/cm²) in the receiver compartment as compared to CBD patches (no MNs), which showed no drug permeation at the end of 48 hours study. Data also showed that CBD MN patches showed significantly higher (P < .0001) permeation with a drug concentration of 838.51 ± 191.74 µg/cm² as compared to CBD patches (no MNs) which showed no drug permeation at the end of 2 hours. Data also showed the flux of 59.60 ± 7.49 µg/cm²/h in the case of CBD MN patches. Whereas, the CBD patch with no MNs showed flux of 0.00 ± 0.00 µg/cm²/h (Fig. 3b).

#### In vivo PK study

PK data demonstrated that CBD MN patches and CBD subcutaneous injection (control) showed maximum systemic concentration (Cmax) of 50.24 ± 15.87 ng/ml and  $55.53 \pm 13.55$  ng/ml systemic absorption, respectively. Tmax was found to be  $2.00 \pm 0.00$  and  $1.00 \pm 0.00$  for CBD MN patches and CBD subcutaneous injection (control), respectively. Further, our studies also showed 1348.96 ± 374.81 (ng/ml\*h) of AUC (0-48 hours) for CBD MN patch and  $932.21 \pm 255.92$  (ng/ml\*h) for CBD patch with no MNs. The relative bioavailability of CBD MN patch was found to be 144.70%, considering CBD subcutaneous injection as standard. At the conclusion of the study, it was noted that the CBD MN patches exhibited strong adherence to the rat's skin. No signs of inflammation or damage were detected on the rat's skin at the conclusion of the study (Fig. 4).

#### In vitro in vivo correlation

To observe the mechanism of release in vitro and ex vivo, a system of first-order, zero-order, and Michaelis-Menten kinetics were tested, and the best-fit model was obtained from a three-parameter combination of burst (i.e. early completion) first-order and sustained zero-order release kinetics (Fig. 5). The first-order burst rate *in vitro* was estimated at Kf = 2.86/hand 3.20/h for the CBD MN and CBD patch (no MNs), respectively. The sustained zero-order percent released over 24 hours from matrix material for both CBD MN and patch (no MNs) was estimated from the model to be approximately the same at 1.62% and 1.61% released each hour, as revealed by parallel release profiles. The ex vivo kinetic fit revealed a much slower burst phase (i.e. Kf = 0.232/h), suggestive of a 90% rate reduction in crossing the skin model and late completion (>12 hours) of first-order release (Kf = 0.232/h or 3 hours half-time).

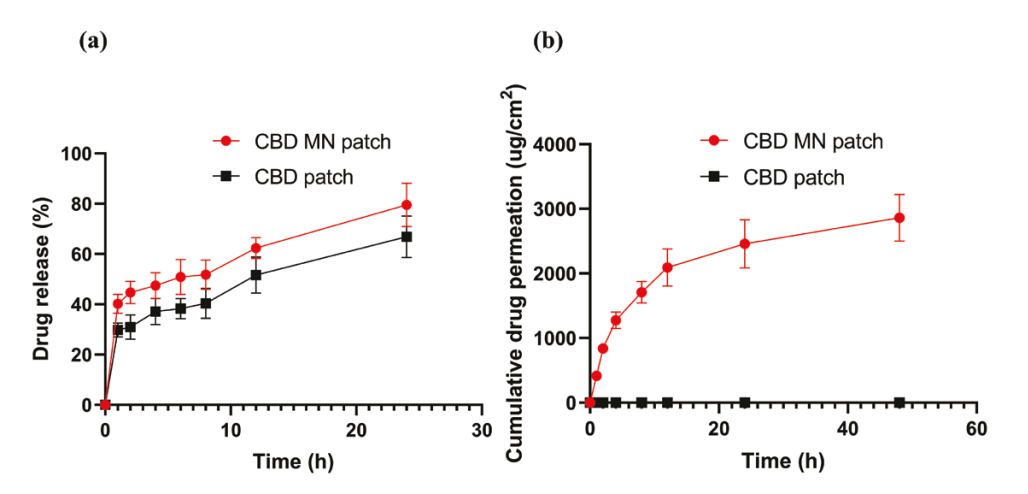


Figure 3. (a) In vitro release study showing increase in drug release in case of cannabidiol microneedle (CBD MN) patch as compared to cannabidiol (CBD) patch (no microneedles) (results are expressed in mean  $\pm$  SD [n = 3], P = ns not significant; (b) Ex vivo permeation study showing enhanced drug permeation from cannabidiol microneedle (CBD MN) patch as compared to CBD patch (no microneedle) (results are expressed in mean  $\pm$  SD [n = 3], \*\*\*\*P < .0001).

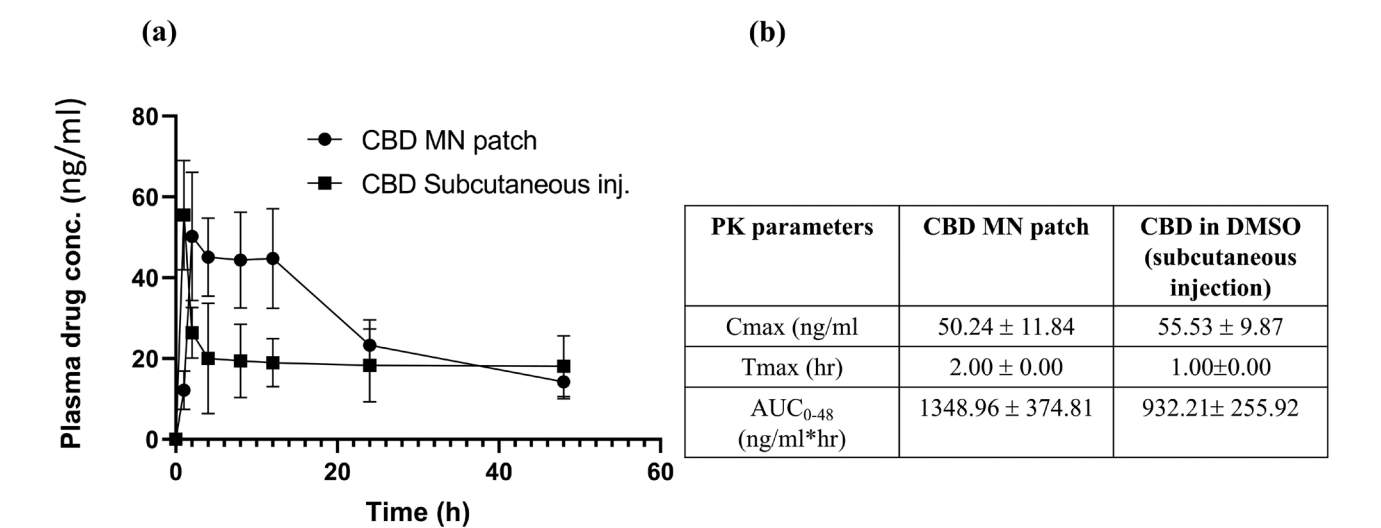
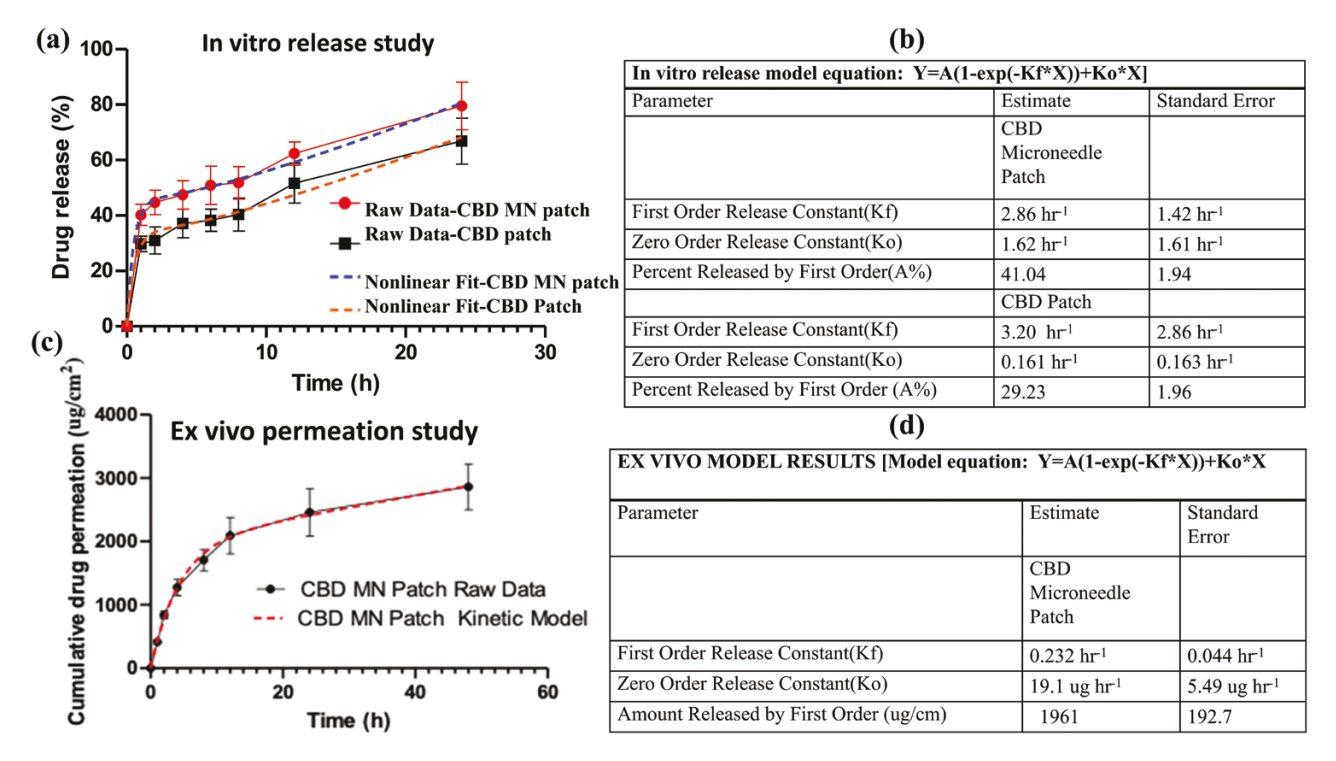


Figure 4. (a) In vivo pharmacokinetic (PK) study showing enhanced bioavailability in case of cannabidiol microneedle (CBD MN) patch as compared to cannabidiol (CBD) patch (no microneedle); (b) PK profile showing increase  $AUC_{0.48}$  in case of cannabidiol microneedle (CBD MN) patch as compared to cannabidiol (CBD) patch (no microneedle) with identical Cmax (results are expressed in mean  $\pm$  SD [n = 4]; \*P < .05).

The *in-vivo* PK data for the CBD MN patch was successfully fit to a first-order absorption–elimination two exponential model plus zero-order input as per the *in-vitro* data, whereas the CBD subcutaneous injection (as a positive control) was

fit to a simple two-compartment exponential model with instantaneous input (Fig. 6a–d). We observed a good kinetic fit with an estimated absorption-limited disposition of CBD MN patch of Ka = 0.062/h or a plasma disposition half-life



**Figure 5**. Release kinetics model fit showing (a) and (b) cannabidiol microneedle (CBD MN) patch and cannabidiol (CBD) patch (no microneedle) in *in vitro* release study with their model results; (c) and (d) cannabidiol microneedle (CBD MN) patch in *ex vivo* permeation study with its model results. \*All data were normalized by volume.

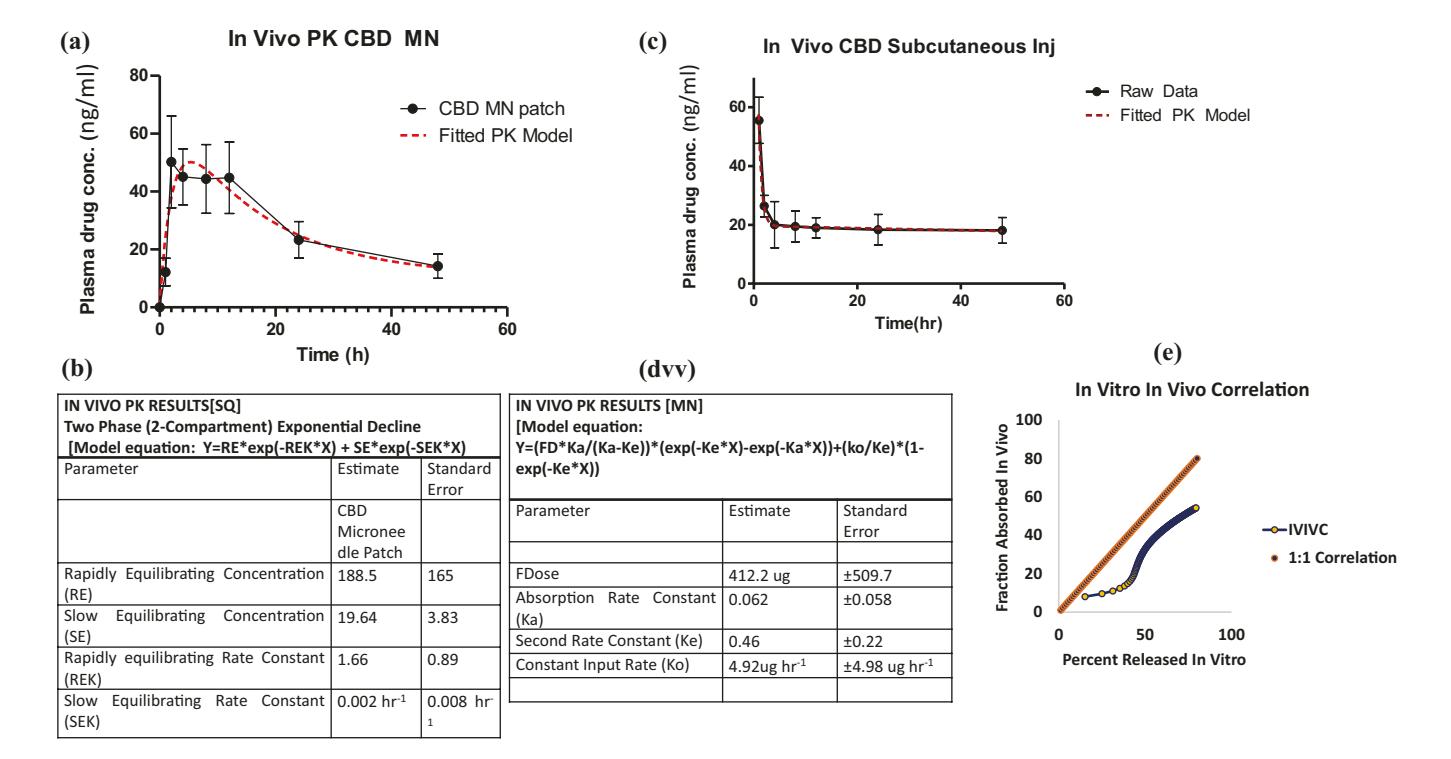


**Figure 6.** Pharmacokinetic model fits and parameters for (a) and (d) CBD MN patch in *in vivo* PK study (c) and (b) CBD subcutaneous injection in *in vivo* PK study, (e) IVIV correlation showing parallel amount of drug released *in vitro* vs fraction absorbed in *in vivo* study. \*All data were normalized by volume.

of approximately 11 hours. The model fits *in vivo* helped confirm the mechanism of release demonstrated *in vitro*, whereas model estimated parameters help to compare formulations in future studies.

Evaluating the kinetic mechanism of release permitted a better understanding of the correlation between the percent released from the CBD MN patch in vitro and the percent absorbed in vivo over the first 24 hours. The IVIVC study comparison of *in-vitro* and *in-vivo* data supported the *ex vivo* results, where the diffusion rates out of the matrix in vitro were faster than in vivo for the first 90 minutes and resulted in a deviation from a one-to-one correlation early in the release profile (i.e. the percent released at each time was not superimposable (Fig. 6e)). This early deviation was expected due to the presence of the sub-dermal skin barrier in vivo. After the initial 90-minute burst period in the dual phase in-vitro release model, the trend in percent released presented a Level A correlation, as it was highly and closely correlated with the percent absorbed (Pearson's R = 0.97, P < .05) as shown in Fig. 6e. Demonstrating a one-to-one correlation between the percent absorbed in vivo and the percent released in vivo, following the initial burst phase, helped validate the functionality of this CBD MN patch in rats.

#### **Discussion**

3D printing has emerged as a valuable technology for fabricating MN patches due to its precision, versatility, and potential for personalized medicine. 3D printing allows for the customization of MN patch designs to meet specific therapeutic needs. Parameters such as needle length, density, shape, and arrangement can be tailored for optimal drug delivery efficiency. The considerable lipophilicity of CBD (with a log P value greater than 5) poses difficulties in its transdermal delivery, primarily due to its limited solubility in water (approximately 2–10 µg/ml in water) [11]. Moreover, CBD has been reported to have low bioavailability when taken orally because of its extensive first-pass metabolism in liver [13]. MN drug delivery would be ideal for delivering CBD transdermally as it disrupts the stratum corneum, which is the main barrier for the drug permeation into the systemic circulation via skin. Previously, we have reported the fabrication of a dissolvable ibuprofen MN patch using 3D DLP printing technology [16]. However, this method has not been used to develop MN patches of other APIs including CBD. Considering the numerous advantages of 3D printing technique, the objective of the present study was to develop dissolvable CBD MN patches using our previously developed 3D printing method and further evaluate them in a PK study. In this study, CBD MN patches (2-day patches) were fabricated with enhanced transdermal permeation with drug flux of  $40.46 \pm 5.02 \,\mu\text{g/cm}^2\text{/h}$  and increased bioavailability (AUC of  $1348.96 \pm 374.81$  (ng/ml\*h)) as compared to control formulation (AUC of  $932.21 \pm 255.92$  (ng/ml\*h)). To the best of our knowledge, this is the first study showing enhanced bioavailability of CBD for 48 hours (2 days) from 3D-printed MN patch as compared to the control (CBD subcutaneous injection).

Our optical microscopic images showed that the optimized resin formulation from our previous study produced CBD MNs with ~800 µm height, ~250 µm base diameter, and ~15 µm tip RoC. This suggests that the developed custom

resin can be used to print the MNs containing various APIs if the API is soluble in resin. Additionally, optimized printing parameters including slice thickness (25 µm), LED current of 125 (5.86 mA/unit), and exposure time in the range of 4–5 seconds could successfully produce CBD MNs like our previously published work on IBU MNs. This indicates that these optimized DLP printing parameters could be used to print MNs containing various APIs.

3D-printed CBD MN patch formed perforations on the human skin when gentle thumb pressure was applied, indicating that the MNs possessed ample strength to breach the stratum corneum layer of the skin. Researchers showed that maltose MNs, when tested for their mechanical resilience on Parafilm M® film, exhibited the ability to create pores, indicating their capacity to penetrate human skin [21]. Moreover, a texture analysis assessing the strength of CBD MNs revealed that there was no deformation in their morphology when subjected to forces of 0.1-0.5 N/MN. This observation implies that the MNs possess sufficient strength for skin penetration. It has been reported that the piercing of the skin by MNs typically requires a force in the range of 25–35 N, depending on the sharpness of the needles [22, 37–39].

*In vitro* release studies showed >50% drug release in 8 hr in both CBD MN patch and CBD patch (no MN). The potential mechanism involved in the dissolution of MNs was the initial enlargement of the microneedles' base diameter due to the absorption of the release medium, primarily because of the porous nature of PEGDAMA. This outcome led to a minor swelling of the MNs, as previously reported in our research [16]. The study also showed an increase in drug release in the case of CBD MN patch as compared to CBD patch with no MN indicating that MNs were first dissolved and released drug as compared to the base of the MN. Nguyen et al., in their work on the fabrication of dissolvable MNs of poly(vinyl alcohol) using the micromolding for doxorubicin transdermal delivery, demonstrated a markedly elevated release of doxorubicin from the dissolving MNs [40]. Additionally, Lim et al. also demonstrated a release study of 3D-printed MN patch developed using vinyl pyrrolidone (VP) and PEGDA and (3:7) resin composition, which exhibited >70% release of an API in the initial 5 hours of the study [41]. In this study, the in vitro release of the MN patch in comparison to a standard patch followed a very predictable two-phase system pattern of first-order burst followed by sustained zero-order release. As would be expected, the impact of increased surface area from the MN cones resulted in a substantial increase in the percent release by first order, and negligible difference in zeroorder release from the matrix. These results (with no change in the overall matrix release rate) suggest that the primary utility of the MN patch would come from adulteration of the stratum corneum by the MNs.

Our results demonstrated that CBD MN patches showed significant (P < .0001) drug permeation as compared to CBD patches (no MNs), which showed no drug permeation at the end of 48 hours study, which suggests that MNs overcome the skin's epidermal stratum corneum layer and the CBD was released in the receptor compartment. On the other hand, CBD patch with no MNs (control), which did not show any skin permeation, indicating that stratum corneum layer was intact. In our study, 3D-printed CBD MN patches showed permeation drug concentration of  $838.51 \pm 191.74 \, \mu g/cm^2$  at

the end of 2 hours, which was higher than work published by other research groups [17, 18]. Ex vivo skin permeation study of micromolded CBD solid dispersion-doped dissolving MNs (Ef/CBD-SD@DMNs) showed cumulative transdermal permeation of ~710 µg/cm<sup>2</sup> CBD at the end of 8 h [17]. Polymer-coated nanoparticles (NPs) MN patch developed using micromolding method showed 59.6 µg/g of CBD release into the brain tissue in an ex vivo study [18]. In the ex vivo test of CBD permeation via the MN patch, the data as a systems check was attempted to be fit to first order release, however, this resulted in a poor fit early in the curve. An attempt of solely zero-order input with a "first order sink" (i.e. the higher the build-up on the ventral surface, the faster its removal). This resulted in a poor fit later in the data. The model was resolved using both the first and zero-order terms from the in vitro experiment, however, the first-order burst was much slower than the in vitro experiment, presumably because the MN cones are protected from a rapid dissolution via the dissolution medium. This resulted in a smooth primarily zero-order input curve in ex vivo performance, and with no discernible lag. This was expected given the very high log P (6.3) of CBD [42]. Because of this highly lipophilic nature, the subcutaneous injection of CBD in vivo behaved like a direct intravenous injection with no absorption phase within the sampling period of 1 hour. Further, the terminal plasma half-life of CBD was exceptionally long in this study, suggestive of a depot effect when giving lipophilic drugs subcutaneously in oil [43, 44].

Evaluation of the CBD formulation via MN patch *in vivo* provided promising results for further investigations as the MN patch results in sustained plasma levels over the 48-hour study period compared to the direct subcutaneous injection. These results were significant and suggest the absorption phase from the MNs is rate controlling against observing a rapid distribution phase decline. In addition to the zero-order input model, here we observe a "flip-flop" phenomenon (i.e. absorption is slow relative to elimination), where actual drug disposition is rate controlled from the MN patch [45].

We further evaluated the correlation between the in vitro release study of CBD and in vivo CBD fraction absorbed for the first 24 hours via Wagner-Nelson method and noncompartmental analysis. The correlation deviated for the first 90 minutes (corresponding to the period of burst release in vitro), and thereafter, the data were well correlated (Pearson's R = 0.97, P < .05). IVIVC was expected given the rate-limiting step in vitro was early burst dissolution of the patch followed by subsequent diffusion-controlled release out of the polymer matrix, whereas in vivo, the use of a highly lipophilic created no further rate-controlling barriers to absorption. Thus, we are able to observe the same trend of release into the media and absorption into the body after 90 minutes. The ability to mimic the *in vivo* absorption behavior of 3D-printed MN patches in vitro should greatly facilitate further research and development of this device for commercial use.

Overall, CBD MN patches were printed using DLP printing technology with optimized parameters. MNs were sharp and mechanically robust MNs to break the skin stratum corneum layer. Additionally, the release study demonstrated that MNs were dissolved and released the drug in release media. Moreover, the skin permeation study showed significantly high drug permeation compared to control CBD

patches. Our *in vivo* PK results showed a significant increase in bioavailability as compared to the control group. Although PEGDAMA 550 polymer and LAP photoinitiator have been reported to be biocompatible and cytocompatible, they are not FDA-approved excipients. Therefore, more studies will be needed to evaluate the biocompatibility and toxicity of these excipients in humans.

#### Conclusion

In summary, sharp and mechanically robust dissolvable CBD MNs were successfully manufactured using novel DLP printing technology. These MNs were dissolved and released drug in skin permeation testing. Our *in vivo* PK study showed enhanced bioavailability with sustained drug release from MN patch in the system circulation as compared to the control group. Our results suggest that the developed resin formulation can also be used to print dissolvable MNs of various APIs using DLP printing. MN preparation using this method can be used for other drugs if the drug is soluble in the resin formulation developed in this study.

## **Author contributions**

Conceptualization, A.B. and M.S.; Experiments, A.B., K.M.K., Software, A.B. and S.S.; Writing—Original Draft Preparation, A.B. and S.S.; Writing—Review & Editing, A.B., S.S. and M.S.; Supervision, M.S. and Funding Acquisition, M.S.

#### **Conflict of interest**

The authors declare that they have no conflict of interest.

# **Funding**

This work was supported by the National Science Foundation-Center of Research Excellence in Science and Technology (NSF-CREST) for Complex Materials Design for Multidimensional Additive Processing (CoManD) award # 1735968 and National Institute on Minority Health and Health Disparities of National Institutes of Health under Award number U54 MD007582 (U54 RCMI grant).

## **Ethical statement**

The animal experiment performed in this study were approved by IACUC, Florida A&M University, Tallahassee, Fl USA. All research were conducted in accordance with this approved protocol (protocol approval no. 019-07 and approval date: May 10, 2021).

#### Data availability

All the data underlying this article are available in the article.

## References

- Prausnitz MR. Microneedles for transdermal drug delivery. Adv Drug Deliv Rev 2004;56:581–7. https://doi.org/10.1016/j. addr.2003.10.023
- Avcil M, Çelik A. Microneedles in drug delivery: progress and challenges. Micromachines 2021;12:1321. https://doi.org/10.3390/ mi12111321

- Singh V, Kesharwani P. Recent advances in microneedles-based drug delivery device in the diagnosis and treatment of cancer. J Control Release 2021;338:394–409. https://doi.org/10.1016/j. iconrel.2021.08.054
- Elahpour N, Pahlevanzadeh F, Kharaziha M et al. 3D printed microneedles for transdermal drug delivery: a brief review of two decades. Int J Pharm 2021;597:120301. https://doi.org/10.1016/j. ijpharm.2021.120301
- Yang Q, Zhong W, Xu L et al. Recent progress of 3D-printed microneedles for transdermal drug delivery. Int J Pharm 2021;593:120106. https://doi.org/10.1016/j.ijpharm.2020.120106
- Li R, Zhang L, Jiang X et al. 3D-printed microneedle arrays for drug delivery. J Control Release 2022;350:933–48. https://doi. org/10.1016/j.jconrel.2022.08.022
- Luzuriaga MA, Berry DR, Reagan JC et al. Biodegradable 3D printed polymer microneedles for transdermal drug delivery. Lab Chip 2018;18:1223–30. https://doi.org/10.1039/c8lc00098k
- Ozyilmaz ED, Turan A, Comoglu T. An overview on the advantages and limitations of 3D printing of microneedles. *Pharm Dev Technol* 2021;26:923–33. https://doi.org/10.1080/10837450.202 1.1965163
- Yadav V, Sharma PK, Murty US et al. 3D printed hollow microneedles array using stereolithography for efficient transdermal delivery of rifampicin. Int J Pharm 2021;605:120815. https://doi.org/10.1016/j.ijpharm.2021.120815
- Sartawi Z, Blackshields C, Faisal W. Dissolving microneedles: applications and growing therapeutic potential. *J Control Release* 2022;348:186–205. https://doi.org/10.1016/j.jconrel.2022.05.045
- 11. Salau O, Bagde A, Kalvala A *et al*. Enhancement of transdermal permeation of cannabinoids and their pharmacodynamic evaluation in rats. *Int J Pharm* 2022;624:122016. https://doi.org/10.1016/j.ijpharm.2022.122016
- Crippa JA, Guimarães FS, Campos AC et al. Translational investigation of the therapeutic potential of cannabidiol (CBD): toward a new age. Front Immunol 2018;9:2009. https://doi.org/10.3389/fimmu.2018.02009
- 13. Millar SA, Stone NL, Yates AS *et al.* A systematic review on the pharmacokinetics of cannabidiol in humans. *Front Pharmacol* 2018;9:1365. https://doi.org/10.3389/fphar.2018.01365
- Millar SA, Maguire RF, Yates AS et al. Towards better delivery of cannabidiol (CBD). Pharmaceuticals (Basel, Switzerland) 2020;13:219. https://doi.org/10.3390/ph13090219
- Grifoni L, Vanti G, Donato R et al. Promising nanocarriers to enhance solubility and bioavailability of cannabidiol for a plethora of therapeutic opportunities. Molecules 2022;27:6070. https://doi.org/10.3390/molecules27186070
- Bagde A, Dev S, Madhavi K Sriram L et al. Biphasic burst and sustained transdermal delivery in vivo using an AI-optimized 3D-printed MN patch. Int J Pharm 2023;636:122647. https://doi. org/10.1016/j.ijpharm.2023.122647
- 17. Shi J, Ma Q, Su W et al. Effervescent cannabidiol solid dispersion-doped dissolving microneedles for boosted melanoma therapy via the "TRPV1-NFATc1-ATF3" pathway and tumor microenvironment engineering. Biomaterials Research 2023;27:48. https://doi.org/10.1186/s40824-023-00390-x
- 18. Muresan P, McCrorie P, Smith F *et al.* Development of nanoparticle loaded microneedles for drug delivery to a brain tumour resection site. *Eur J Pharm Biopharm* 2023;182:53–61. https://doi.org/10.1016/j.ejpb.2022.11.016
- Care, I.o.L.A.R.C.o. and U.o.L. Animals, Guide for the care and use of laboratory animals. US Department of Health and Human Services, Public Health Service, National, 1986.
- Council N.R. Guide for the care and use of laboratory animals. 2010.
- Nguyen HX, Banga AK. Fabrication, characterization and application of sugar microneedles for transdermal drug delivery. *Therapeutic delivery* 2017;8:249–64. https://doi.org/10.4155/tde-2016-0096

- 22. Migdadi EM, Courtenay AJ, Tekko IA *et al.* Hydrogel-forming microneedles enhance transdermal delivery of metformin hydrochloride. *J Control Release* 2018;285:142–51. https://doi.org/10.1016/j.jconrel.2018.07.009
- 23. Johnson AR, Caudill CL, Tumbleston JR *et al.* Single-step fabrication of computationally designed microneedles by continuous liquid interface production. *PLoS One* 2016;11:e0162518. https://doi.org/10.1371/journal.pone.0162518
- Suppasrivasuseth J, Bellantone RA, Plakogiannis FM et al. Permeability and retention studies of (-) epicatechin gel formulations in human cadaver skin. Drug Dev Ind Pharm 2006;32:1007–17. https://doi.org/10.1080/03639040600599889
- Bagde A, Patel K, Kutlehria S et al. Formulation of topical ibuprofen solid lipid nanoparticle (SLN) gel using hot melt extrusion technique (HME) and determining its anti-inflammatory strength.
   Drug Deliv Transl Res 2019;9:816–27. https://doi.org/10.1007/s13346-019-00632-3
- Boakye CH, Patel K, Doddapaneni R et al. Ultra-flexible nanocarriers for enhanced topical delivery of a highly lipophilic antioxidative molecule for skin cancer chemoprevention. Colloids Surf B 2016;143:156–67. https://doi.org/10.1016/j. colsurfb.2016.03.036
- Bagde A, Patel K, Mondal A et al. Combination of UVB absorbing titanium dioxide and quercetin nanogel for skin cancer chemoprevention. AAPS PharmSciTech 2019;20:1–12.
- 28. Jantharaprapap R, Stagni G. Effects of penetration enhancers on in vitro permeability of meloxicam gels. *Int J Pharm* 2007;343:26–33. https://doi.org/10.1016/j.ijpharm.2007.04.011
- 29. Fulzele SV, Babu RJ, Ahaghotu E *et al*. Estimation of proinflammatory biomarkers of skin irritation by dermal microdialysis following exposure with irritant chemicals. *Toxicology* 2007;237:77–88. https://doi.org/10.1016/j.tox.2007.05.005
- 30. McCrudden MT, Alkilani AZ, McCrudden CM *et al.* Design and physicochemical characterisation of novel dissolving polymeric microneedle arrays for transdermal delivery of high dose, low molecular weight drugs. *J Control Release* 2014;180:71–80. https://doi.org/10.1016/j.jconrel.2014.02.007
- 31. Bagde A, Patel K, Kutlehria S *et al.* Formulation of topical ibuprofen solid lipid nanoparticle (SLN) gel using hot melt extrusion technique (HME) and determining its anti-inflammatory strength. *Drug Deliv Transl Res* 2019;9:816–27. https://doi.org/10.1007/s13346-019-00632-3
- 32. Abo-EL-Sooud, K., Absolute and relative bioavailability, in Drug discovery and evaluation: methods in clinical pharmacology. Switzerland: Springer, 2020, 879–85.
- Corporation, W. OASIS Sample extraction 2020. https://www. waters.com/webassets/cms/library/docs/720005685en.pdf (April 2020, date last accessed).
- Guideline, I.H.T. Validation of analytical procedures: text and methodology. 2005. https://database.ich.org/sites/default/files/ Q2%28R1%29%20Guideline.pdf (November 2005, date last accessed).
- 35. Zhang Y, Huo M, Zhou J *et al.* PKSolver: An add-in program for pharmacokinetic and pharmacodynamic data analysis in Microsoft Excel. *Comput Methods Programs Biomed* 2010;99:306–14. https://doi.org/10.1016/j.cmpb.2010.01.007
- Wagner JG, Nelson E. Kinetic analysis of blood levels and urinary excretion in the absorptive phase after single doses of drug. *J Pharm Sci* 1964;53:1392–403. https://doi.org/10.1002/jps.2600531126
- Larrañeta E, Moore J, Vicente-Pérez EM et al. A proposed model membrane and test method for microneedle insertion studies. Int J Pharm 2014;472:65–73. https://doi.org/10.1016/j. ijpharm.2014.05.042
- 38. Lutton RE, Moore J, Larrañeta E *et al*. Microneedle characterisation: the need for universal acceptance criteria and GMP specifications when moving towards commercialisation. *Drug Deliv Transl Res* 2015;5:313–31. https://doi.org/10.1007/s13346-015-0237-z

Cheung K, Han T, Das DB. Effect of force of microneedle insertion on the permeability of insulin in skin. J Diabetes Sci Technol 2014;8:444–52. https://doi.org/10.1177/1932296813519720

- Nguyen HX, Bozorg BD, Kim Y et al. Poly (vinyl alcohol) microneedles: fabrication, characterization, and application for transdermal drug delivery of doxorubicin. Eur J Pharm Biopharm 2018;129:88–103. https://doi.org/10.1016/j.ejpb.2018.05.017
- 41. Lim SH, Kathuria H, Amir MHB et al. High resolution photopolymer for 3D printing of personalised microneedle for transdermal delivery of anti-wrinkle small peptide. J Control Release 2021;329:907–18. https://doi.org/10.1016/j.jconrel. 2020.10.021
- 42. Odi R, Bibi D, Wager T et al. A perspective on the physicochemical and biopharmaceutic properties of marketed antiseizure

- drugs—From phenobarbital to cenobamate and beyond. *Epilepsia* 2020;61:1543–52. https://doi.org/10.1111/epi.16597
- Zuidema J, Kadir F, Titulaer HAC et al. Release and absorption rates of intramuscularly and subcutaneously injected pharmaceuticals (II). Int J Pharm 1994;105:189–207. https://doi.org/10.1016/0378-5173(94)90103-1
- 44. Weng Larsen S, Larsen C. Critical factors influencing the in vivo performance of long-acting lipophilic solutions—impact on in vitro release method design. AAPS J 2009;11:762–70. https://doi. org/10.1208/s12248-009-9153-9
- 45. Yáñez JA, Remsberg CM, Sayre CL *et al.* Flip-flop pharma-cokinetics-delivering a reversal of disposition: challenges and opportunities during drug development. *Ther Deliv* 2011;2:643–72. https://doi.org/10.4155/tde.11.19